# Nano-analytical investigation of the forming process in an HfO2-based resistive switching memory

Gauthier Lefevre, Tristan Dewolf, Nicolas Guillaume, Serge Blonkowski, Christelle Charpin-Nicolle, Eric Jalaguier, Etienne Nowak, Nicolas Bernier, Tom Blomberg, Marko Tuominen, et al.

▶ **To cite this version:**

Gauthier Lefevre, Tristan Dewolf, Nicolas Guillaume, Serge Blonkowski, Christelle Charpin-Nicolle, et al.. Nano-analytical investigation of the forming process in an HfO2-based resistive switching memory. Journal of Applied Physics, 2021, 130 (24), pp.244501. 10.1063/5.0072343 . hal-03720298

**HAL Id: hal-03720298**
**https://hal.science/hal-03720298**

Submitted on 11 Jul 2022

**HAL** is a multi-disciplinary open access archive for the deposit and dissemination of scientific research documents, whether they are published or not. The documents may come from teaching and research institutions in France or abroad, or from public or private research centers.

L'archive ouverte pluridisciplinaire **HAL**, est destinée au dépôt et à la diffusion de documents scientifiques de niveau recherche, publiés ou non, émanant des établissements d'enseignement et de recherche français ou étrangers, des laboratoires publics ou privés.

# Nano-analytical investigation of the forming process in an $HfO_2$-based resistive switching memory

Gauthier Lefevre,[1] Tristan Dewolf,[2] Nicolas Guillaume,[1] Serge Blonkowski,[2] Christelle Charpin-Nicolle,[2] Eric Jalaguier,[2] Etienne Nowak,[2] Nicolas Bernier,[2] Tom Blomberg,[3, a)] Marko Tuominen,[3] Hessel Sprey,[4] Guillaume Audoit,[2] and Sylvie Schamm-Chardon[5]

[1)] *Univ. Grenoble Alpes, CNRS, CEA-LETI Minatec, LTM, 38054 Grenoble, France*

[2)] *Univ. Grenoble Alpes, CEA, Leti, F-38000 Grenoble, France*

[3)] *ASM Microchemistry, Pietari Kalmin katu 3 F 2, 00560 Helsinki, Finland*

[4)] *ASM Belgium, Kapeldreef 75, 3001 Leuven, Belgium*

[5)] *Univ. Toulouse, CNRS, CEMES, 29 rue Jeanne Marvig, F-31055 Toulouse, France*

(*Electronic mail: sylvie.schammchardon@cemes.fr)

(Dated: 10 November 2021)

Metal oxide based Resistive Random Access Memory (RRAM) devices are highly attractive candidates for next-generation nonvolatile memories, but the resistive switching phenomena remains poorly understood. This article focuses on the microscopic understanding of the initial forming step, which is decisive for the switching process. The integrated resistive switching memory effect in Ti/$HfO_2$/TiWN MIM structures is studied. After forming, transmission electron microscopy (TEM) investigations pointed out the presence of a funnel-shaped region, in the ON state of the cell, where slightly oxidized Ti (TiOx) was present within $HfO_2$ dielectric. Modelling of the measured On state conductance of the cell with the semi-classical approximation is consistent with a conductive nanometric TiOx filament (or a sum of sub-nanometric TiOx filaments) present in the funnel shaped region. The conductive area is likely formed by diffusion after the dielectric breakdown.

## I. INTRODUCTION

Resistive switching memory is an emerging technology and highly promising for next generation memory devices and neuromorphic computing[1–3]. Among these, transition-metal-oxide-based RRAM is under consideration because of its promising performances in terms of scalability, switching speed, endurance, energy efficiency and NMOS-friendly integration[4,5]. RRAM is seen as a very attractive solution to design downscaled ultra-low-power devices for new applications such as neuromorphic systems or in-memory computing[6–10].

This technology is based on a resistance transition obtained by applying suitable electrical pulses on metal oxides. The choice of proper materials (electrodes as well as metal oxide) in the Metal Insulator Metal (MIM) configuration is a key issue for fabrication and electrical operation since it leads to various behaviours[11–13].

Several models to explain the electrical behaviour of the devices have been proposed. They are based on the assumption that a major role in the switching resistance is played by charged species, such as positively charged O vacancies[14–18]. However, the physics triggering the resistance switching is still uncertain, as experimental evidence not only supports switching due to oxygen vacancies[19,20] but also to metallic migration from the electrodes[21,22] and to Schottky emission and/or hopping conduction mechanisms at the electrode-dielectric interfaces[23]. To overcome limitations in the development of such memories like switching variability and retention tail losses, a deep understanding of physical phenomena arising across the dielectric solid-state material appears to be essential. If clear evidence of the role of oxygen and vacancies in the oxide-based insulator has been demonstrated, impact of the electrodes nature and electrode-dielectric interface still remains to be understood.

$HfO_2$ is one of the most suitable dielectric candidate for RRAM technology since it has the advantage of being more mature from a technological point of view, is widely studied and presenting an ease from the integration point of view[24–26]. Concerning electrodes, titanium is commonly used in the current memory manufacturing processes and presents interesting properties (corrosion-resistance and high chemical activity).

Nonetheless, the role of TiN/Ti electrodes is controversial. Ti induces the formation of an interface layer enriched with O vacancies, which could be responsible for the bipolar switching, could reduce forming and set voltages, and improve retention ; anyway, this could also impede the reset, reduce the endurance and smooth the switching procedure.[13,23,27]

Considerable TEM reports on resistive memories have been proposed, with a range of different techniques, including off-axis electron holography for electrostatic potential mapping[20] and energy dispersive X-ray spectroscopy for elemental analysis[28]. Among these advanced TEM techniques, it was found that Electron Energy Loss Spectroscopy (EELS) was the most appropriate tool for assessing changes during the switching process.[29] Indeed, to provide relevant information concerning the redox-based ion-migration related switching processes, it's necessary to measure quantitative changes in atomic concentration and electronic states of involved elements with sufficient spatial resolution, which is possible by EELS in the transmission electron microscope. It should be noted that for this purpose, core-loss EELS, directly connected to elemental concentration and electronic structure, is

[a)] currently with Aalto University.

more reliable than low-loss EELS which is indirectly sensitive to chemical composition and more delocalized[30].

In this article, a chemical investigation of $HfO_2$-based Resistive Random Access Memory (RRAM) integrated with a Ti top electrode and a TiWN bottom electrodes is performed based on TEM-EELS. Quantitative physicochemical information is obtained on the observed nanometer-scale conductive paths. Balance between the role played by oxygen and metal (Ti-Hf) atoms is discussed and a two-step interpretation of the forming process is proposed. Results provide appealing details for further improvement.

## II. EXPERIMENTAL SECTION

A resistive memory (6400 µm$^2$) comprising a 10 nm Back-End-of-Line thick $HfO_2$ deposited by Atomic Layer Deposition (ALD), then 10 nm of Physical Vapor Deposited (PVD) Ti and 50 nm of PVD TiN as top electrode, is schematically illustrated in Figure 1. The bottom electrode is grown by ALD and consists of a layer of TiWN[31]. In this work, studied bitcells were integrated in series with NMOS transistors, enabling a 1 mA current control. 1T-1R single devices were investigated in more detail.

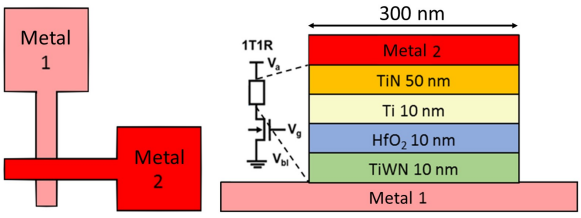


FIG. 1. Schematic top view and cross-section (along the dotted line) of the 1T-1R stack, the TEM lamella was extracted within the crossing area of Metal 1 and Metal 2.

Electrical programming and measurements were carried out using a cascade microtech bench working with a Keithley 4200 Source Meter unit, with the bottom electrode being grounded. When switching from the OFF to the ON state, the current was limited to 0.3 mA (compliance current) to avoid the breakdown of the samples. A TEM lamella was extracted at the crossing of Metal 1 and Metal 2, which had a size of 0.09 µm$^2$. The TEM lamella was prepared using Focus Ion Beam etching and polishing utilizing an FEI dual-beam Helios 450S. Rough milling was applied using an operating voltage of 30 kV with subsequent reductions to 8 keV, 5 keV and finally 2 keV to obtain a compromise between reducing the surface damage and keeping a high quality parallel-sided lamella. The final thickness of the lamella is 50 to 60 nm over a few micrometers length. Before TEM examination, the sample was cleaned with an oxygen-argon plasma to remove hydrocarbon contamination. The morphological and analytical investigations of the stack were performed using a double-aberration-corrected FEI Titan Ultimate TEM equipped with a high brightness electron source working at an acceleration voltage of 300 keV, and with a Gatan Quantum energy filter working in the Dual EELS mode (simultaneous acquisition of low-loss and core-loss EELS spectra). High Angle Annular Dark field images (HAADF) were used to localize the area of interest for the analysis. EELS spectra and maps were obtained with an energy resolution of 1.2 eV and a spatial resolution at the nanometer scale. Quantitative elemental maps were obtained using standard EELS signal integration of a denoised signal obtained after a post-acquisition treatment[32]. Intensities in the maps present the relative volumetric concentration of each element (Ti, N, O and Hf), obtained after correction and with reference to stoichiometric TiN and $HfO_2$ within a pristine stack. Note that the pristine lamella has been extracted from another unstressed RRAM device with the same procedure as the TEM lamella obtained after forming.

## III. RESULTS AND DISCUSSION

### A. Electrical characterizations

Extensive electrical characterizations were performed on bitcells. The numerous memory cells tested present clear forming, reset and set events. For reliability of results, endurance tests were performed, demonstrating the devices remained functional even after $10^4$ cycles (fig. 2, also denoting that the forming step is non-destructive. Characteristics for integration, such as endurance and retention time over long periods, not addressed here, have been presented in previous work.[33]

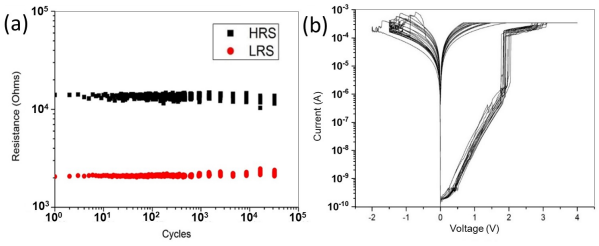


FIG. 2. Endurance measurements : clear set, reset (a) and cycling (b) events are observed, indicating proper forming operation.

To initiate switching, a preliminary forming operation is required. In our case, a linear positive voltage ramp was applied on the top electrode, the bottom one being grounded. As it is shown on figure 2(b) and 3, the current increased exponentially until 2 V. At this voltage, the abrupt current increase corresponded to the $HfO_2$ dielectric breakdown. After this step, the current reached the compliance value, which was low enough to allow the switching observation in the negative part of the current voltage characteristics. Note that the forming step at 2 V was followed by a second breakdown (at about 2.7 V), which was an artifact due to the architecture including a parallel resistance, detailed in[34]. It is worth noting that the current voltage characteristics after forming is linear (insert of figure 3) and this point will be explained in the discussion section.

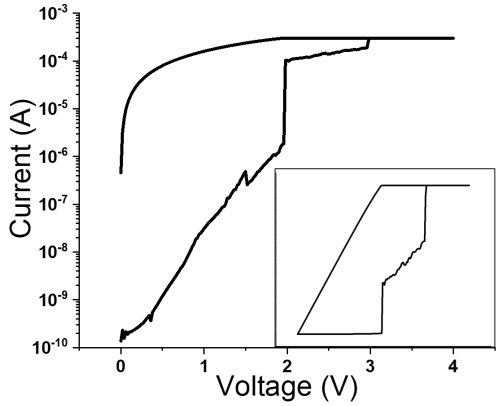


FIG. 3. I-V characteristics for quasi-static forming step up to 4 V (forming step with linear scale in inset).

### B. TEM characterizations

After the forming operation, a lamella has been extracted from the region in between metal 1 and 2 electrodes as indicated in figure 1. The HAADF image of the thinned lamella is shown in figure 4. In such an image, intensity is proportional to the atomic number of the elements so that the heavy elements appear brighter than the light ones. In particular, the $HfO_2$ layer is brighter than the TiWN one, which is brighter than the Ti, TiN, metal 1 and metal 2. Two localized irregularities in the intensity were observed mainly within the $HfO_2$ brighter layer at the positions defined by the dotted rectangles (noted area 1 and 2 in figure 4), which suggests a possible modification of element distribution. Outside these areas, the stack is still homogeneous, with well-defined and planar interfaces.

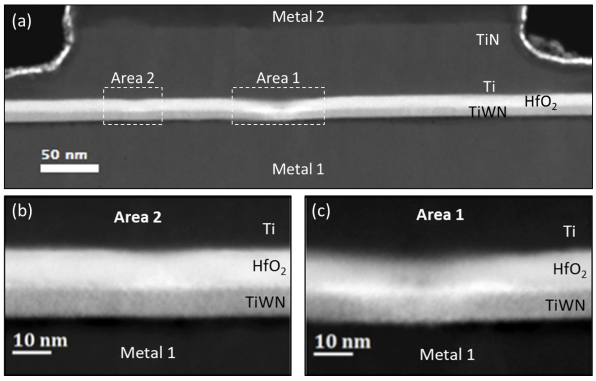


FIG. 4. HAADF image of the device after the forming step : two modified regions are within dotted rectangles (a) and shown enlarged in (b) and (c).

EELS elemental maps of N, Ti, O and Hf in area 1 were compared with those obtained in a pristine stack as shown in figure 5 (Hf map not registered in the pristine stack). Interfaces were relatively abrupt compositionally in the pristine stack, which was not the case in the central part of area 1, where diffusion of elements is clearly evidenced. An oxygen-titanium interdiffusion is observed at the top of the dielectric layer, whereas hafnium migrated in the TiWN electrode. Elemental profiles were taken perpendicularly to the layers in the switched stack at the border as well as in its central part, providing complementary information (fig. 6). In addition to the diffusions already mentioned in the maps, two important aspects need to be discussed. First, O is also present with Hf in the TiWN bottom electrode but with a low concentration that leads to a Hf-rich place. Thus, O profile tends to diffuse mainly toward the top electrode as Hf seems to diffuse toward the bottom electrode as also evidenced in the sections obtained for different depths in the stack as shown on figure 7 (g and h cases). Moreover, Ti is present not only in the upper part of the dielectric but it also connects to the bottom electrode. Places where this occurs can be found by looking at the rainbow map of Ti where yellow traces are seen within the red dielectric forming a funnel-shaped envelope. More quantitatively, this is evidenced with Ti profiles (green) extracted from sections obtained for different depths in the stack as shown on figure 7 (c to f cases). Thus, Ti diffuses from the top electrode to the bottom electrode consistently with conductive atomic force microscopy (C-AFM) observations[35].

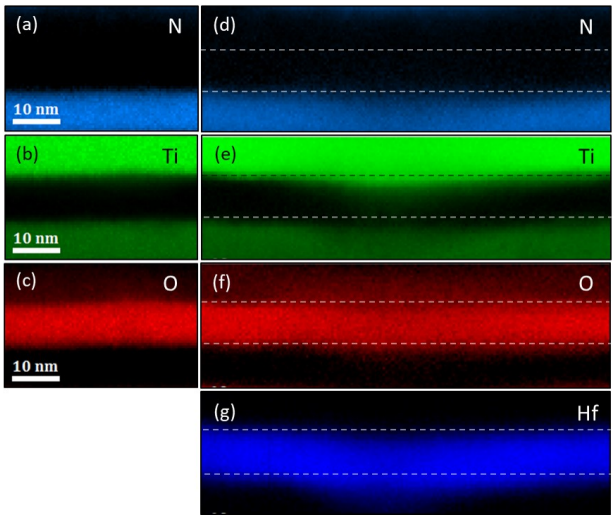


FIG. 5. EELS elemental maps of N (a) and (d), Ti (b) and (e) and O (c) and (f) in a pristine stack and in area 1 respectively. Hf map in area 1 (g).

The way Ti is connected within the $HfO_2$ layer should be approached studying the Energy-Loss Near-Edge Structures (ELNES) at the onset of the Ti$-L_{2,3}$ and O-K edges obtained from the funnel-shaped area. If the Ti$-L_{2,3}$ fine structures of Ti and oxides can be of help interpreting fingerprint, this is not the case for O-K ones in $HfO_2$. Indeed, a thorough investigation of the published work showed that these are very sensitive to the crystallisation state of $HfO_2$ (amorphous or not)[36], to the phase in which it crystallizes (monoclinic or tetragonal)[37] and to the presence of dopant and O vacancies[38]. It is not possible to distinguish between the different contributions, the major modifications being gathered over 10 eV within the

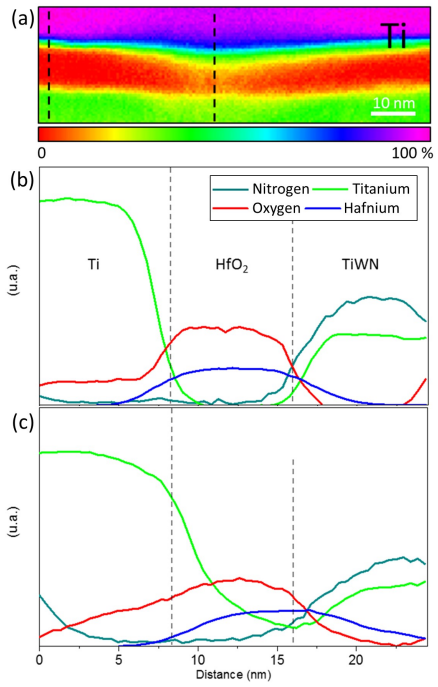


FIG. 6. EELS rainbow map of Ti in the switched stack (a) and two elemental profiles obtained perpendicular to the layers, outside the center (b) and in the center (c) along the dashed lines drawn on (a).

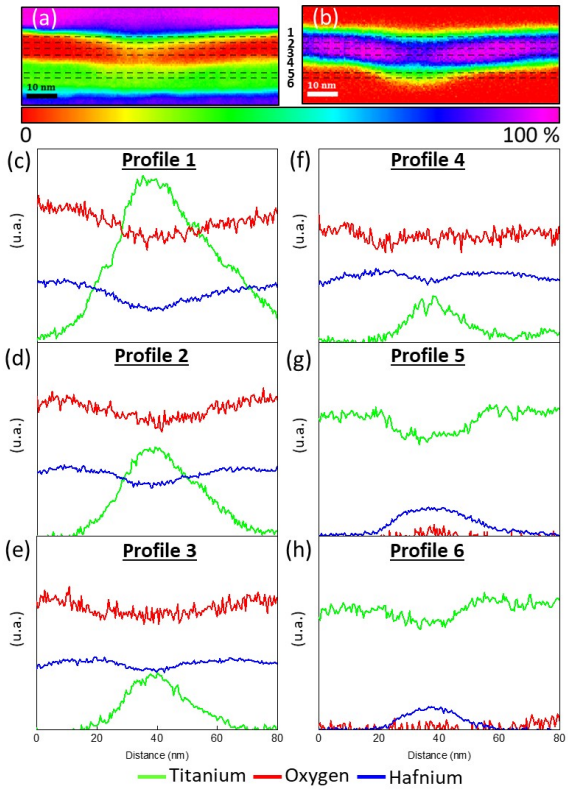


FIG. 7. EELS rainbow maps in the switched stack of Ti (a) and Hf (b) and 6 profiles (c to h) obtained parallel to the interfaces at different depths in the $HfO_2$ layer and the bottom electrode at the positions of the dashed lines in (a).

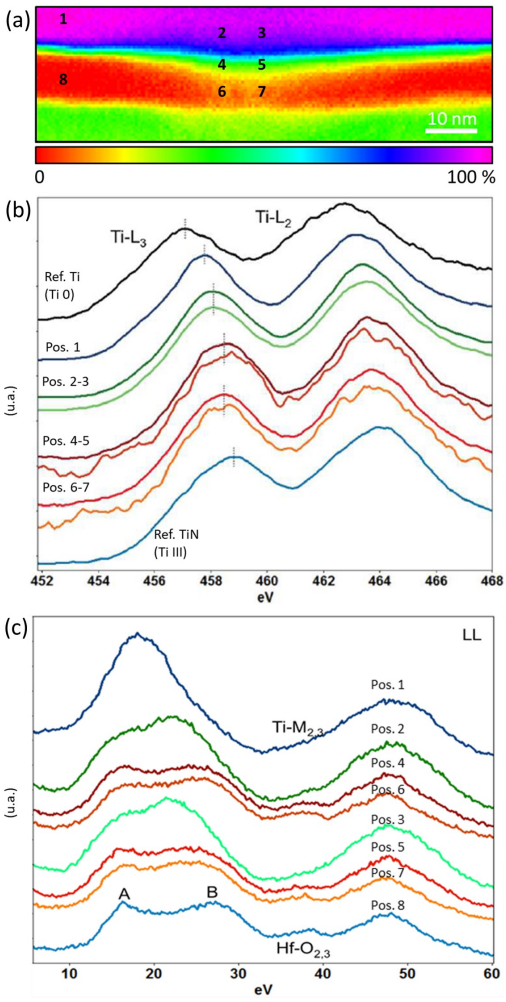


FIG. 8. EELS rainbow map of Ti in the switched stack where analyzed positions are indicated (1 to 8) (a), Ti-L2,3 ELNES for the positions 1 to 7 with added ELNES of Ti and TiN as references (b) and corresponding Low-Loss spectra, with the one of pure $HfO_2$ (position 8) (c).

same small range of energy. On the Ti$-L_{2,3}$ ELNES side, the fine structures are quite simpler to investigate. Two main peaks describe the first 10 eV of the Ti$-L_{2,3}$ ELNES arising through the transition of 2p core electrons to the narrow unoccupied transition metal d states. The $L_3$ transition from the $2p_{3/2}$ level is the lowest in energy, followed by the $L_2$ transition from the $2p_{1/2}$ state. The shape and the position of these 2 peaks are dependent on the Ti coordination (site geometry) and valence states. For example, the $L_{2,3}$ onset shifts to higher energy with increasing oxidation state in Ti oxides[39,40] and nitrides[41]. Moreover, for Ti oxides with Ti valences III and above, like in $Ti_2O_3$ (III) and $TiO_2$ (IV), the ligand-field due to the octahedral coordination of Ti causes the separation in 2 peaks of each $L_3$ and $L_2$ signatures due to the split of the 5d states in the conduction band in the two-fold $e_g$ and the three-fold $t_{2g}$ states[40,42]. In figure 8 (b), ELNES of the Ti$-$L edge are shown for different positions in the stack as indicated by numbers on the Ti rainbow map. They correspond to a $3 \times 5$

$nm^2$ area analyzed around each position. Looking at the Ti state in the top electrode, outside (pos. 1) and above the funnel shaped area (pos. 2 and 3), one can see that the position of the maximum of the $L_3$ peak is shifted towards higher energies by 0.7 and 1 eV compared to the one of pure Ti (obtained with similar conditions and added on the figure for reference). This corresponds to O/Ti ratios of 0.1 and 0.3 respectively, thus suggesting a slight oxidation, which is more pronounced above the funnel shaped as already observed in the O map of fig.5. Within the funnel (pos. 4 to 7), $Ti-L_{2,3}$ ELNES shapes are not modified and are similar whatever the position considered with 2 main peaks but further shifted towards higher energies with respect to pure Ti (1.4 eV). However, the peak shift is less than for a Ti with valence III like in TiN (obtained with similar conditions and added to the figure for reference). On the basis of these comparisons, one can estimate the valence of Ti to be less than III when present within $HfO_2$. The Low-Loss (LL) spectra corresponding to the $Ti-L_{2,3}$ ELNES signatures are also shown in figure 8 (c). Signatures at positions 1 and 2/3 are consistent with a slightly oxidized Ti with, respectively, a small shift of the main peak by 0.3 eV with respect to the value for pure Ti (pos. 1)[43] and the beginning of the splitting of this peak (pos.2/3) as observed but in a much more pronounced way for titanium oxides TiO (valence II) to $TiO_2$ (valence IV)[44]. Going inside the funnel area (pos. 4 to 7), the LL signatures can be described at a first approximation as the weighted sum of the LL signatures of $HfO_2$ (pos. 8) and partially oxidized Ti ( as depicted in pos. 2/3). Note that the $HfO_2$ characteristic signature preserved there excludes the presence of O-deficient $HfO_2$ or Hf, these having different low-loss signatures (basically one large main peak located around 22 eV)[21,37,45].

### C. Discussion

Advanced TEM analysis presented here highlights numerous interesting observations. After forming operation, two damaged areas appeared in the TEM lamella extracted from a 1T-1R stack. The memory cell was modified at these places and for one of them (area 1), a funnel-shaped area containing partially oxidized Ti and $HfO_2$ was observed. Moreover, O diffusion towards the top electrode and O depletion of $HfO_2$ at the bottom electrode were also evidenced. Similar phenomena were observed for area 2 but with a much limited extent. These observations are in favor of a conduction path connecting the top and bottom electrodes made of a conductive $TiO_x$ phase within a $HfO_2$ matrix, relayed by an O deficient $HfO_y$ phase at the bottom electrode.

The TEM observation of a funnel-shaped area has a consequence on the conduction. The smallest part of the funnel near the bottom electrode constitutes a constriction. The area of this constriction limits the current. Since this constriction has a small size (around 10 nm in diameter from figure 7) compared to an electronic mean free path, it is reasonable to consider the semi-classical approximation of quantum conductance instead of the classic Ohm's law. The temperature independence of the conductance demonstrated in similar OxRRAMs (4 K to 300 K range[46]) and the linear current voltage characteristic as seen in the insert of figure 3 ($I_{on} = G_{on}.V$ with $G_{on} = 1.5 \times 10^{-4}$ S) support the use of the Sharvin conductance given by[47,48]:

$$G_{on} = \frac{2q^2}{h}\frac{k_F^2 S_c}{4\pi} \quad (1)$$

In equation (1), $q$ is the electron charge, $h$ is the Planck constant, $k_F$ the Fermi wave vector and $S_c$ the constriction section (supposed to be a disk of diameter $d$). The first fraction in equation (1) represents the quantum conductance and the second approximates the number of conduction channels.

As deduced previously $TiO_x$ is likely at the origin of the OxRRAM On state conduction after the forming process. Let us consider if this is reasonable. If $TiO_x$ had the Ti properties, the corresponding Fermi wave vector $k_F = 1.52 \times 10^{10}\ m^{-1}$ would correspond to a constriction section diameter of 5 Å. Now, considering $TiO_x$ with a much lower electronic density than Ti, $n \sim 1 \times 10^{21}\ cm^{-3}$, in the framework of free electron model $k_F$ is now equal to $k_F = (3\pi^2 n)^{1/3} = 3 \times 10^9\ m^{-1}$, which leads to a section diameter of 1.8 nm. If we remind that the volume of the funnel contains both $TiO_x$ and $HfO_2$, the constriction area 10 nm in size could be considered as discontinuous thus Sc could be the sum of several smaller conductive areas, resulting in the same conductance.

One can now formulate assumptions on the forming scenario leading to this funnel. The first step is the dielectric breakdown that consists in the appearance of a conduction path in the dielectric. This step, common to all dielectrics and semiconductors[49], arises in our case at around 2 V (figures 2b and 3). The conduction path may be attributed to several phenomena in the dielectric submitted to a high electric field (Zener effect, electron avalanche, chemical bond breaking). In this conduction path, the current density is very high. For the 300 µA in figure 2(b) the current density is $3 \times 10^{-10}\ A\,cm^{-2}$ for a 1 nm filament section. Note that several conduction paths can be initiated. However, all the current flow only in one of them limiting the effect on the others. In this conduction path and its vicinity, because of Joule heating, the temperature can increase considerably. Therefore, a thermally activated diffusion becomes likely and the diffusion force which have the direction opposite to the atom concentration gradient (figure 5 b & c) pushes Ti atoms from top to bottom electrode. It is this region, which is observable with TEM and not the initial conduction path. Note that in the second region (area 2 in figure 4), the effect is drastically reduced, likely because the current flows mostly in the area 1, expected to be the place of the first breakdown. In the case of oxygen, the concentration spread consistently with diffusion law in the region where the temperature is high. Note also that an electrical field induced drift of Ti positive ions is also possible. During the forming, the top electrode is positively biased, thus the force acting on Ti atoms from top electrode that could be ionized is directed toward the bottom electrode. However, according to[35] the switching characteristics remains the same whatever the forming polarization. For this reason it seems that diffusion, in the case discussed here, is more likely than drift.

It's worth noting that switching mechanisms arising and

observed in this work are intimately linked to the experimental procedure and the memory cell studied (i.e. Ti/$HfO_2$ (10 nm)/TiWN MIM configuration with its proper shape, dimensions and crystalline state) where each characteristic plays a relevant role.

## IV. CONCLUSIONS

In this paper, a large set of TEM analyses (Z-contrast imaging, spatially-resolved EELS elemental maps, ELNES fingerprint) coupled with electrical measurements have been used and the results thoroughly discussed in order to elucidate the forming mechanism in an NMOS integrated $HfO_2$-based resistive switching memory with Ti/TiWN electrodes. After forming, for the first time demonstrated using core-loss EELS elemental maps, a Ti-rich funnel-like region appears, which can be linked to a conductive filament within the $HfO_2$ dielectric. The measured On state conductance was compared in the framework of a semi classical approximation and is consistent with the smallest size of the funnel in the vicinity of the bottom electrode. A two-step forming scenario consisting in dielectric breakdown followed by diffusion may explain the funnel aspect of the conductive region. Such a new insight is essential to a deeper understanding of the physics of the subsequent switching processes. Also, it helps improving the device reliability, which is desirable for technological implementation of $HfO_2$-based RRAM, a highly attractive candidate for next generation nonvolatile memories.

## CONFLICTS OF INTEREST

There are no conflicts to declare.

## ACKNOWLEDGEMENTS

This work was partially performed at the Platform For NanoCharacterization (PFNC) of CEA-Leti with support from the Recherche Technologique de Base (RTB) of the french ministery of research. This work has been partially supported by European commission, French State and Auvergne-Rhône Alpes region through the funding of ECSEL 621217 PANACHE and 783176 WAKeMeUP Projects part of IPCEI (Important Project of Common European Interest) on microelectronics and French Nano2022 program.

## DATA AVAILABILITY STATEMENT

The data that support the findings of this study are available from the corresponding author upon reasonable request.

[1] A. Sawa, "Resistive switching in transition metal oxides," Materials Today **11**, 28–36 (2008).

[2] D. S. Jeong, R. Thomas, R. S. Katiyar, J. F. Scott, H. Kohlstedt, A. Petraru, and C. S. Hwang, "Emerging memories: resistive switching mechanisms and current status," Reports on Progress in Physics **75**, 076502 (2012).

[3] T.-C. Chang, K.-C. Chang, T.-M. Tsai, T.-J. Chu, and S. M. Sze, "Resistance random access memory," Materials Today **19**, 254–264 (2016).

[4] H.-S. P. Wong, H.-Y. Lee, S. Yu, Y.-S. Chen, Y. Wu, P.-S. Chen, B. Lee, F. T. Chen, and M.-J. Tsai, "Metal–oxide RRAM," Proceedings of the IEEE **100**, 1951–1970 (2012).

[5] J. J. Yang, D. B. Strukov, and D. R. Stewart, "Memristive devices for computing," Nature Nanotechnology **8**, 13–24 (2012).

[6] S. Park, J. Noh, M. lae Choo, A. M. Sheri, M. Chang, Y.-B. Kim, C. J. Kim, M. Jeon, B.-G. Lee, B. H. Lee, and H. Hwang, "Nanoscale RRAM-based synaptic electronics: toward a neuromorphic computing device," Nanotechnology **24**, 384009 (2013).

[7] M. A. Zidan, J. P. Strachan, and W. D. Lu, "The future of electronics based on memristive systems," Nature Electronics **1**, 22–29 (2018).

[8] A. Benoist, S. Blonkowski, S. Jeannot, S. Denorme, J. Damiens, J. Berger, P. Candelier, E. Vianello, H. Grampeix, J. F. Nodin, E. Jalaguier, L. Perniola, and B. Allard, "28nm advanced cmos resistive ram solution as embedded non-volatile memory," in *2014 IEEE International Reliability Physics Symposium* (2014) pp. 2E.6.1–2E.6.5.

[9] T. Hirtzlin, M. Bocquet, B. Penkovsky, J.-O. Klein, E. Nowak, E. Vianello, J.-M. Portal, and D. Querlioz, "Digital biologically plausible implementation of binarized neural networks with differential hafnium oxide resistive memory arrays," Frontiers in Neuroscience **13** (2020), 10.3389/fnins.2019.01383.

[10] M. K. Mahadevaiah, E. Perez, C. Wenger, A. Grossi, C. Zambelli, P. Olivo, F. Zahari, H. Kohlstedt, and M. Ziegler, "Reliability of cmos integrated memristive $HfO_2$ arrays with respect to neuromorphic computing," in *2019 IEEE International Reliability Physics Symposium (IRPS)* (2019) pp. 1–4.

[11] F. Pan, S. Gao, C. Chen, C. Song, and F. Zeng, "Recent progress in resistive random access memories: Materials, switching mechanisms, and performance," Materials Science and Engineering: R: Reports **83**, 1–59 (2014).

[12] H.-Y. Chen, S. Brivio, C.-C. Chang, J. Frascaroli, T.-H. Hou, B. Hudec, M. Liu, H. Lv, G. Molas, J. Sohn, S. Spiga, V. M. Teja, E. Vianello, and H.-S. P. Wong, "Resistive random access memory (RRAM) technology: From material, device, selector, 3d integration to bottom-up fabrication," Journal of Electroceramics **39**, 21–38 (2017).

[13] C. Cagli, J. Buckley, V. Jousseaume, T. Cabout, A. Salaun, H. Grampeix, J. F. Nodin, H. Feldis, A. Persico, J. Cluzel, P. Lorenzi, L. Massari, R. Rao, F. Irrera, F. Aussenac, C. Carabasse, M. Coue, P. Calka, E. Martinez, L. Perniola, P. Blaise, Z. Fang, Y. H. Yu, G. Ghibaudo, D. Deleruyelle, M. Bocquet, C. Muller, A. Padovani, O. Pirrotta, L. Vandelli, L. Larcher, G. Reimbold, and B. de Salvo, "Experimental and theoretical study of electrode effects in $HfO_2$ based RRAM," in *2011 International Electron Devices Meeting* (IEEE, 2011).

[14] R. Waser, R. Dittmann, G. Staikov, and K. Szot, "Redox-based resistive switching memories - nanoionic mechanisms, prospects, and challenges," Advanced Materials **21**, 2632–2663 (2009).

[15] D. Ielmini, "Modeling the universal set/reset characteristics of bipolar RRAM by field- and temperature-driven filament growth," IEEE Transactions on Electron Devices **58**, 4309–4317 (2011).

[16] S. Larentis, F. Nardi, S. Balatti, D. C. Gilmer, and D. Ielmini, "Resistive switching by voltage-driven ion migration in bipolar RRAM—part II: Modeling," IEEE Transactions on Electron Devices **59**, 2468–2475 (2012).

[17] M. Bocquet, D. Deleruyelle, H. Aziza, C. Muller, J.-M. Portal, T. Cabout, and E. Jalaguier, "Robust compact model for bipolar oxide-based resistive switching memories," IEEE Transactions on Electron Devices **61**, 674–681 (2014).

[18] N. Xu, B. Gao, L. Liu, B. Sun, X. Liu, R. Han, J. Kang, and B. Yu, "A unified physical model of switching behavior in oxide-based RRAM," in *2008 Symposium on VLSI Technology* (IEEE, 2008).

[19] P. Calka, E. Martinez, V. Delaye, D. Lafond, G. Audoit, D. Mariolle, N. Chevalier, H. Grampeix, C. Cagli, V. Jousseaume, and C. Guedj, "Chemical and structural properties of conducting nanofilaments in TiN/$HfO_2$-based resistive switching structures," Nanotechnology **24**, 085706 (2013).

[20] C. Li, B. Gao, Y. Yao, X. Guan, X. Shen, Y. Wang, P. Huang, L. Liu, X. Liu, J. Li, C. Gu, J. Kang, and R. Yu, "Direct observations of nanofilament evolution in switching processes in $HfO_2$-based resistive random access memory by in situ TEM studies," Advanced Materials **29**, 1602976 (2017).

[21] S. Privitera, G. Bersuker, B. Butcher, A. Kalantarian, S. Lombardo, C. Bongiorno, R. Geer, D. Gilmer, and P. Kirsch, "Microscopy study of the con-

ductive filament in $HfO_2$ resistive switching memory devices," Microelectronic Engineering **109**, 75–78 (2013).

[22] K. Pey, N. Raghavan, W. H. Liu, X. Wu, K. Shubhakar, and M. Bosman, "Real-time analysis of ultra-thin gate dielectric breakdown and recovery - a reality," in *Proceedings of the 20th IEEE International Symposium on the Physical and Failure Analysis of Integrated Circuits (IPFA)* (IEEE, 2013).

[23] K.-J. Zhou, T.-C. Chang, C.-Y. Lin, C.-K. Chen, Y.-T. Tseng, H.-X. Zheng, H.-C. Chen, L.-C. Sun, C.-Y. Lien, Y.-F. Tan, C.-W. Wu, Y.-H. Yeh, and S. M. Sze, "Abnormal high resistive state current mechanism transformation in Ti/$HfO_2$/TiN resistive random access memory," IEEE Electron Device Letters **41**, 224–227 (2020).

[24] H. Y. Lee, P. S. Chen, T. Y. Wu, Y. S. Chen, C. C. Wang, P. J. Tzeng, C. H. Lin, F. Chen, C. H. Lien, and M.-J. Tsai, "Low power and high speed bipolar switching with a thin reactive ti buffer layer in robust $HfO_2$ based RRAM," in *2008 IEEE International Electron Devices Meeting* (IEEE, 2008).

[25] G. Bersuker, D. C. Gilmer, D. Veksler, P. Kirsch, L. Vandelli, A. Padovani, L. Larcher, K. McKenna, A. Shluger, V. Iglesias, M. Porti, and M. Nafría, "Metal oxide resistive memory switching mechanism based on conductive filament properties," Journal of Applied Physics **110**, 124518 (2011).

[26] B. Govoreanu, G. Kar, Y.-Y. Chen, V. Paraschiv, S. Kubicek, A. Fantini, I. Radu, L. Goux, S. Clima, R. Degraeve, N. Jossart, O. Richard, T. Vandeweyer, K. Seo, P. Hendrickx, G. Pourtois, H. Bender, L. Altimime, D. Wouters, J. Kittl, and M. Jurczak, "$10 \times 10$ nm$^2$ Hf/$HfO_x$ crossbar resistive ram with excellent performance, reliability and low-energy operation," in *2011 International Electron Devices Meeting* (IEEE, 2011).

[27] P. Gonon, M. Mougenot, C. Vallée, C. Jorel, V. Jousseaume, H. Grampeix, and F. E. Kamel, "Resistance switching in $HfO_2$ metal-insulator-metal devices," Journal of Applied Physics **107**, 074507 (2010).

[28] G. Niu, M. A. Schubert, S. U. Sharath, P. Zaumseil, S. Vogel, C. Wenger, E. Hildebrandt, S. Bhupathi, E. Perez, L. Alff, M. Lehmann, T. Schroeder, and T. Niermann, "Electron holography on $HfO_2$/$HfO_{2-x}$bilayer structures with multilevel resistive switching properties," Nanotechnology **28**, 215702 (2017).

[29] D. Cooper, C. Baeumer, N. Bernier, A. Marchewka, C. L. Torre, R. E. Dunin-Borkowski, S. Menzel, R. Waser, and R. Dittmann, "Anomalous resistance hysteresis in oxide ReRAM: Oxygen evolution and reincorporation revealed by in situ TEM," Advanced Materials **29**, 1700212 (2017).

[30] R. F. Egerton, "Electron energy-loss spectroscopy in the TEM," Reports on Progress in Physics **72**, 016502 (2008).

[31] T. Blomberg, M. Tuominen, and H. Sprey, "Nanocrystalline $Ti_xW_yN_z$ thin films deposited by atomic layer deposition," in *2014 Baltic ALD conference* (Helsinki, 2014).

[32] P. Trebbia and N. Bonnet, "EELS elemental mapping with unconventional methods i. theoretical basis: Image analysis with multivariate statistics and entropy concepts," Ultramicroscopy **34**, 165–178 (1990).

[33] M. Azzaz, E. Vianello, B. Sklenard, P. Blaise, A. Roule, C. Sabbione, S. Bernasconi, C. Charpin, C. Cagli, E. Jalaguier, S. Jeannot, S. Denorme, P. Candelier, M. Yu, L. Nistor, C. Fenouillet-Beranger, and L. Perniola, "Endurance/retention trade off in $HfO_x$ and $TaO_x$ based rram," in *2016 IEEE 8th International Memory Workshop (IMW)* (2016) pp. 1–4.

[34] N. Guillaume, M. Azzaz, S. Blonkowski, E. Jalaguier, P. Gonon, C. Vallée, T. Blomberg, M. Tuominen, H. Sprey, S. Bernasconi, C. Charpin-Nicolle, and E. Nowak, "Improvement of HRS Variability in OxRRAM by Tailored Metallic Liner," in *2019 International Conference on Solid State Devices and Materials* (JSAP, Nagoya University, Aichi, Japan, 2019).

[35] A. K. Singh, S. Blonkowski, and M. Kogelschatz, "Resistive switching study in $HfO_2$ based resistive memories by conductive atomic force microscopy in vacuum," Journal of Applied Physics **124**, 014501 (2018), https://doi.org/10.1063/1.5025143.

[36] G. D. Wilk and D. A. Muller, "Correlation of annealing effects on local electronic structure and macroscopic electrical properties for $HfO_2$ deposited by atomic layer deposition," Applied Physics Letters **83**, 3984–3986 (2003).

[37] S. U. Sharath, S. Vogel, L. Molina-Luna, E. Hildebrandt, C. Wenger, J. Kurian, M. Duerrschnabel, T. Niermann, G. Niu, P. Calka, M. Lehmann, H.-J. Kleebe, T. Schroeder, and L. Alff, "Control of switching modes and conductance quantization in oxygen engineered $hfo_x$based memristive devices," Advanced Functional Materials **27**, 1700432 (2017).

[38] X. F. Wang, Q. Li, and M. S. Moreno, "Effect of al and y incorporation on the structure of $HfO_2$," Journal of Applied Physics **104**, 093529 (2008).

[39] M. Yoshiya, I. Tanaka, K. Kaneko, and H. Adachi, "First principles calculation of chemical shifts in ELNES/NEXAFS of titanium oxides," Journal of Physics: Condensed Matter **11**, 3217–3228 (1999).

[40] E. Stoyanov, F. Langenhorst, and G. Steinle-Neumann, "The effect of valence state and site geometry on $Ti-L_{3,2}$ and $O-K$ electron energy-loss spectra of $Ti_xO_y$ phases," American Mineralogist **92**, 577–586 (2007).

[41] S. Terada, K. Asayama, M. Tsujimoto, H. Kurata, and S. Isoda, "Chemical shift of electron energy-loss near-edge structure on the nitrogen k-edge and titanium l3-edge at TiN/Ti interface," Microscopy and Microanalysis **15**, 106–113 (2009).

[42] C. Mitterbauer, G. Kothleitner, and F. Hofer, "Comparative electron energy-loss near-edge fine structure investigations of titanium oxides," Microscopy and Microanalysis **9**, 834–835 (2003).

[43] Y. Kihn, C. Mirguet, and L. Calmels, "EELS studies of Ti-bearing materials and ab initio calculations," Journal of Electron Spectroscopy and Related Phenomena **143**, 117–127 (2005).

[44] M. Bosman, M. Watanabe, D. Alexander, and V. Keast, "Mapping chemical and bonding information using multivariate analysis of electron energy-loss spectrum images," Ultramicroscopy **106**, 1024–1032 (2006).

[45] J. H. Jang, H.-S. Jung, J. H. Kim, S. Y. Lee, C. S. Hwang, and M. Kim, "Investigation of oxygen-related defects and the electrical properties of atomic layer deposited $HfO_2$ films using electron energy-loss spectroscopy," Journal of Applied Physics **109**, 023718 (2011).

[46] S. Blonkowski and T. Cabout, "Bipolar resistive switching from liquid helium to room temperature," Journal of Physics D: Applied Physics **48**, 345101 (2015).

[47] M. Brandbyge, J. Schio/tz, M. R. So/rensen, P. Stoltze, K. W. Jacobsen, J. K. No/rskov, L. Olesen, E. Laegsgaard, I. Stensgaard, and F. Besenbacher, "Quantized conductance in atom-sized wires between two metals," Physical Review B **52**, 8499–8514 (1995).

[48] M. J. M. de Jong, "Transition from sharvin to drude resistance in high-mobility wires," Physical Review B **49**, 7778–7781 (1994).

[49] S. Lombardo, J. H. Stathis, B. P. Linder, K. L. Pey, F. Palumbo, and C. H. Tung, "Dielectric breakdown mechanisms in gate oxides," Journal of Applied Physics **98**, 121301 (2005).

[50] R. Waser, R. Dittmann, G. Staikov, and K. Szot, "Redox-based resistive switching memories - nanoionic mechanisms, prospects, and challenges," Advanced Materials **21**, 2632–2663 (2009), https://onlinelibrary.wiley.com/doi/pdf/10.1002/adma.200900375.

[51] T. Dewolf, V. Delaye, N. Bernier, D. Cooper, N. Chevalier, H. Grampeix, C. Charpin, E. Jalaguier, M. Kogelschatz, S. Schamm-Chardon, and G. Audoit, "Nano-characterization of switching mechanism in $HfO_2$-based oxide resistive memories by TEM-EELS-EDS," in *The 16th European Microscopy Congress* (2016).

[52] K. L. Pey, R. Thamankar, M. Sen, M. Bosman, N. Raghavan, and K. Shubhakar, "Understanding the switching mechanism in rram using in-situ tem," in *2016 IEEE Silicon Nanoelectronics Workshop (SNW)* (2016) pp. 36–37.

[53] D. Cooper, C. Baeumer, N. Bernier, A. Marchewka, C. L. Torre, R. E. Dunin-Borkowski, S. Menzel, R. Waser, and R. Dittmann, "Anomalous resistance hysteresis in oxide ReRAM: Oxygen evolution and reincorporation revealed by in situ TEM," Advanced Materials **29**, 1700212 (2017).

[54] S. Dirkmann, J. Kaiser, C. Wenger, and T. Mussenbrock, "Filament growth and resistive switching in hafnium oxide memristive devices," ACS Applied Materials & Interfaces **10**, 14857–14868 (2018), pMID: 29601180, https://doi.org/10.1021/acsami.7b19836.

[55] M. Cancarevic, M. Zinkevich, and F. Aldinger, "Thermodynamic description of the ti-o system using the associate model for the liquid phase," Calphad **31**, 330 – 342 (2007).

[56] M. P. Agustin, L. R. C. Fonseca, J. H. Hooker, and S. Stemmer, "HAADF imaging and low-loss EELS investigation of $HfO_2$/TiN interfaces in high-k gate stacks," Microscopy and Microanalysis **11** (2005), 10.1017/s1431927605504458.

[57] P. Calka, E. Martinez, V. Delaye, D. Lafond, G. Audoit, D. Mariolle, N. Chevalier, H. Grampeix, C. Cagli, V. Jousseaume, and C. Guedj, "Chemical and structural properties of conducting nanofilaments in TiN/$HfO_2$-based resistive switching structures," Nanotechnology **24**, 085706 (2013).

[58] C. Li, Y. Yao, X. Shen, Y. Wang, J. Li, C. Gu, R. Yu, Q. Liu, and M. Liu, "Dynamic observation of oxygen vacancies in hafnia layer by in situ transmission electron microscopy," Nano Research **8**, 3571–3579 (2015).
[59] J. L. Murray and H. A. Wriedt, "The o-ti (oxygen-titanium) system," Journal of Phase Equilibria **8**, 148–165 (1987).
[60] E. Stoyanov, F. Langenhorst, and G. Steinle-Neumann, "The effect of valence state and site geometry on Ti $-L_{2,3}$ and $O_K$ electron energy-loss spectra of $Ti_xO_y$ phases," American Mineralogist **92**, 577–586 (2007).
[61] R. Waser and M. Aono, "Nanoionics-based resistive switching memories," Nature Materials **6**, 833–840 (2007).